Probing the skyrmion phase of MnSi through the field-exponent of the isothermal entropy change

Tapas Samanta [1,*] Chris Taake [1] and Luana Caron [1,2]
[1] Faculty of Physics, Bielefeld University, P.O. Box 100131, D-33501 Bielefeld, Germany
[2] Helmholtz-Zentrum Berlin für Materialien und Energie, Berlin 12489, Germany

(Received 16 January 2025; revised 14 May 2025; accepted 9 June 2025; published 26 June 2025)

A detailed study of the field-induced entropy change evolution under hydrostatic pressure (p) of the well-known skyrmion-hosting MnSi system was carried with the goal of assessing its magnetocaloric properties and identifying the skyrmion phase. The pressure-induced modification of the first-order phase transition boundary of the skyrmion phase in MnSi has been determined through the field-exponent, $n(T, B)$, of the isothermal entropy change [$\Delta S \alpha (B)^n$]. The skyrmion phase boundaries generated from $n(T, B)$ and ac-susceptibility data are in qualitatively good agreement at *ambient pressure*. The application of hydrostatic pressure can lower the transition temperature of MnSi towards the hydrogen liquefaction temperature (~20 K) while retaining the first-order nature of the phase transition up to the highest applied pressure of $p = 9.8$ kbar. As a result, the studied system maintains good magnetocaloric properties near 20 K [$|\Delta S| = 4.24$ J/kg K, adiabatic temperature change $|\Delta T_{ad}| = 4.62$ K (estimated), and refrigerant capacity $|RC| = 91.37$ J/kg for $\Delta B = 7$ T with $p = 9.8$ kbar], which are comparable to those of light rare-earth Laves phase compounds with the added benefit of being composed of cheap and abundant elements.

DOI: 10.1103/1ftc-3xyw

I. INTRODUCTION

For over a decade, the helimagnetic B20 compound MnSi has been intensively studied due to its tendency to form a magnetic skyrmion lattice induced by low magnetic field [1,2]. Topologically protected nano-sized skyrmions behave like particles [3] and have enormous potential for ultradense information storage and advanced spintronics applications due to lower energy consumption compared to existing technologies [4]. At lower field, MnSi exhibits two magnetic phase transitions in tandem: a fluctuation-induced first-order phase transition to a helical ordered (HM) state around $T_C \sim 29$ K followed by a second-order transition from a fluctuation-disordered (FD) to the paramagnetic (PM) state around $T_F \sim 30$ K [5–10]. Moreover, several field-induced magnetic states can be stabilized in MnSi depending on temperature and applied magnetic field, resulting in a very rich magnetic phase diagram [5,7,10,11]. Extensive studies have been carried out with the objective of accurately identifying the nature of the different magnetic phases [such as HM, FD, skyrmion, conical, and field-polarized (FP)] with a special emphasis on the skyrmion phase and the order of phase transitions between different phases [5,7,10]. Among the different experimental techniques, very specialized ones such as real-space Lorentz transmission electron microscopy [12], small-angle neutron scattering in reciprocal space [1], and the neutron spin-echo technique [13] have been used to detect the skyrmion phase. However, the signature of the skyrmion phase can also be identified indirectly from lab-based measurements, e.g., ac-susceptibility [11], Hall effect [14], specific heat [10], magnetoelectric effect [15], and magnetostriction [16]. Bauer *et al.* [10] identified the order of phase transitions among the different magnetic phases based on precise specific-heat measurements of MnSi. In their study, it was found that the phase boundary associated with the skyrmion phase is first-order in nature. Moreover, a tricritical point (TCP) was also identified in the phase diagram of MnSi.

In addition to the potential for spintronics applications, inexpensive MnSi also exhibits quite a large magnetocaloric effect (MCE) around 30 K, making it an attractive candidate for cryogenic magnetic refrigeration applications [17]. Furthermore, the skyrmion phase signature has been examined based on entropic considerations [18]. A field-induced increase of the isothermal entropy change (ΔS is positive upon cooling cycle) has been observed inside the skyrmion phase, similar to that which is commonly observed in antiferromagnetic systems below the critical field value of the metamagnetic transition [19]. A discontinuous change of ΔS has been reported for skyrmion hosting materials $MnSi_{0.962}Al_{0.038}$ and $Fe_{0.7}Co_{0.3}Si$, which is taken as a sign that the skyrmion phase transition is first-order in nature [20]. In the present study, we have determined the order of the skyrmion phase transition in the skyrmion-hosting MnSi system based on the value of the field-exponent (n) of the isothermal entropy change [$\Delta S \alpha (B)^n$]. Recently, a quantitative criterion for identifying the order of magnetic phase transitions was developed by Law *et al.* [21]. According to this criterion, $n^{max} > 2$ signifies a first-order phase transition.

*Contact author: tapas.sinp@gmail.com

Interestingly, the criterion can identify first-order phase transitions irrespective of materials class.

It is already well established that the application of hydrostatic pressure (p) can lower the phase transition temperature of MnSi [22,23]. Based on this earlier observation, a study of the hydrostatic pressure-dependent MCE near hydrogen liquefaction temperature (~20 K) has been carried out. Interestingly, application of p can effectively tune the phase transition temperature while maintaining relatively large ΔS and refrigerant capacity (RC).

II. METHODS

A conventional arc-melting technique under an ultrahigh-purity Ar atmosphere was employed to prepare a polycrystalline MnSi sample by taking the constituent elements Mn and Si of purity better than 99.9%. The as-cast sample was annealed at 850 °C for 7 days inside an evacuated quartz tube under an inert atmosphere (~200 mbar backfilled Ar). A Philips X'Pert Pro MPD diffractometer with a Cu $K\alpha$ radiation source was used to measure x-ray diffraction (XRD) on a powder sample at room temperature. The structural refinement of the XRD data was carried out using Rietveld's refinement method as implemented in the FullProf software [24]. The dc-magnetization and ac-susceptibility measurements were performed using a Quantum Design MPMS 3 magnetometer. A home-made BeCu piston-cylinder pressure cell was used to execute the magnetic measurements under hydrostatic pressure (p). Mineral oil was used as the pressure-transmitting medium. Based on the pressure-induced shift of the superconducting transition temperature of Sn (used as a reference manometer, $T_C \sim 3.72$ K at ambient pressure and field of approximately 0.0005 T [25]), the values of the applied pressure (p) were determined. The isothermal entropy change (ΔS) was calculated from isofield $M(T)$ using a Maxwell relation as described by Caron *et al.* [26].

III. RESULTS AND DISCUSSION

The Rietveld refinement profile of the room-temperature XRD data for MnSi is shown in Fig. 1. The system crystallizes in the B20 cubic structure (space group $P2_13$), which is consistent with earlier reports [1,2]. The estimated lattice parameter as obtained from the Rietveld refinement of the XRD data is $a = 4.5592\,(4)$ Å at room temperature.

The hydrostatic pressure (p) induced variation of the temperature-dependent dc-magnetization (M) under a 0.01 T applied magnetic field is shown in Fig. 2(a). Two consecutive magnetic phase transitions have been observed (T_C and T_F) as previously reported [5–10]. T_C (~28 K) is connected to the first-order phase transition between HM and FD states, whereas the second-order phase transition at T_F (~30 K) is associated with a transformation between FD and PM states. With increasing p, T_C progressively decreases and shifts about 9.5 K with the application of $p = 9.6$ kbar. The observed shift in T_C towards lower temperature for MnSi is consistent with earlier results and can be explained as a destabilization of the long-range helical order resulting from the pressure-induced increase of the itinerant electron character of the magnetism [27]. As expected for itinerant electron magnetism, the saturation magnetization decreases with increasing p due to the pressure-induced enhancement of the itinerant character [shown in Fig. 2(b)].

The temperature-dependent isothermal entropy change (ΔS) at ambient pressure as well as under hydrostatic pres-

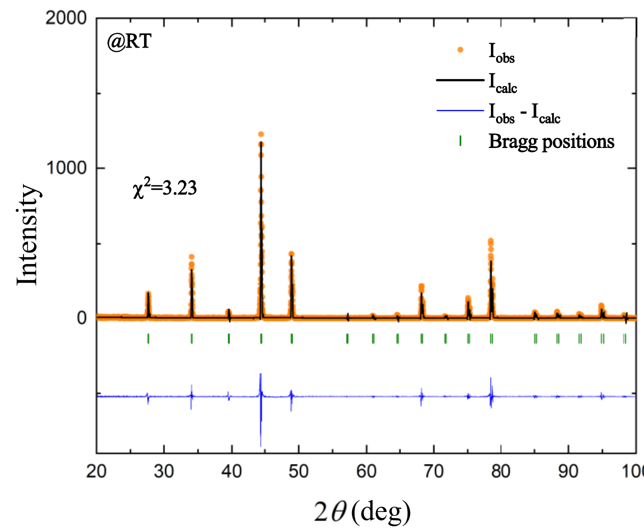

FIG. 1. Rietveld refinement of the room-temperature XRD data for MnSi.

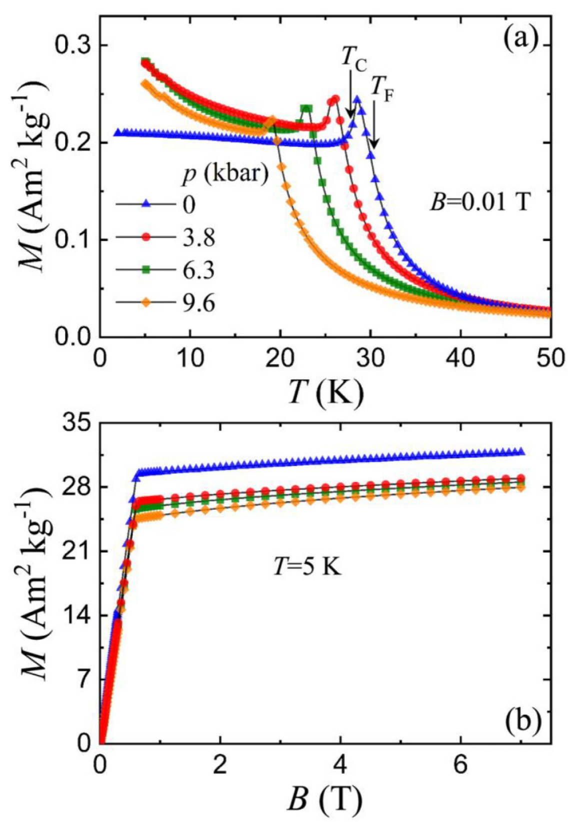

FIG. 2. (a) Magnetization (M) as a function of temperature during heating in the presence of 0.01 T magnetic field and different applied hydrostatic pressures (p). (b) Field dependence of isothermal magnetization at 5 K for different p.

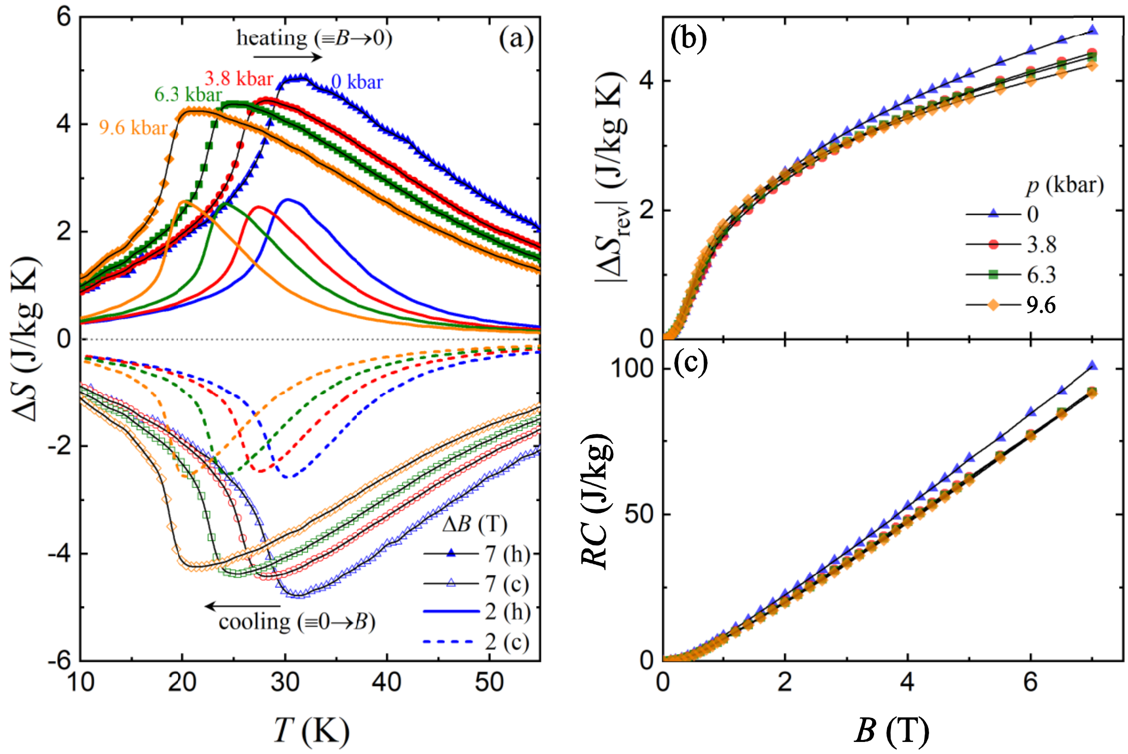

FIG. 3. (a) Entropy change (ΔS) as a function of temperature during heating and cooling for $\Delta B = 2$ and 7 T in the presence of different applied hydrostatic pressure (p). (b) Field dependence of reversible entropy change ($|\Delta S_{\rm rev}|$) for different p. (c) Refrigerant capacity (RC) as a function of the magnetic field as estimated for different p.

sure (p) during heating and cooling are shown in Fig. 3(a) for $\Delta B = 2$ and 7 T. The details of $\Delta S(T)$ for all applied field values can be found in the Supplemental Material (S1) [28]. A conventional MCE (ΔS is positive during heating or upon removal of the magnetic field) has been observed at higher field with a $\Delta S(T)$ peak near the FD-PM transition at $T_{\rm F}$. Instead of a gradual change in $\Delta S(T)$ as observed above $T_{\rm F}$ in the PM state, a sharp change of ΔS has been realized near $T_{\rm C}$, reflecting the first-order transition between FD and successive low-temperature magnetic phases (e.g., HM) at low field ($B < 0.4$ T). The maximum $|\Delta S|$ at ambient pressure reaches a value of about 4.83 J/kg K for $\Delta B = 7$ T, which is consistent with the earlier report (4.18 J/kg K for $\Delta B = 7$ T) [17]. Although the maximum value of $|\Delta S|$ is moderate, MnSi has the potential to exhibit a relatively large adiabatic temperature change ($\Delta T_{\rm ad} = 5.26$ K for $\Delta B = 7$ T) as reported by Arora *et al.* [17]. Due to the decrease of the phase transition temperature with increasing hydrostatic pressure, the peak position of the $\Delta S(T)$ curve shifts to a lower temperature. For $p = 9.6$ kbar, $\Delta S(T)$ shows a peak around the hydrogen liquefaction temperature (~20 K) with a maximum $|\Delta S| = 4.24$ J/kg K for $\Delta B = 7$ T, which is about 12% lower than the ambient pressure value. Recalculating the value of $\Delta T_{\rm ad}$ by considering the value of T/c [c is specific heat, which connects the ΔS and $\Delta T_{\rm ad}$ as $\Delta T_{\rm ad} = -(T/c)\Delta S$ [29]] remains constant with increasing p; $\Delta T_{\rm ad}$ is estimated to reach 4.62 K for $\Delta B = 7$ T and $p = 9.6$ kbar. Considering the estimated magnetocaloric parameters (ΔS and $\Delta T_{\rm ad}$), the magnetocaloric properties of MnSi are comparable to those of light rare-earth Laves phase compounds [30]. Furthermore, MnSi consists of cheaper, nontoxic, and abundant elements, which is advantageous for applications. $|\Delta S|$ is almost fully reversible [$|\Delta S_{\rm rev}|$ was estimated based on the peak value of the overlap region of the $|\Delta S(T)|$ curves during heating and cooling], as shown in Fig. 3(b). Notice that the value of $|\Delta S_{\rm rev}|$ in the low field region (around 1 T) is higher for higher pressure, which is most likely associated with the stronger magnetic field sensitivity of the magnetization resulting from the pressure-induced softening of the magnetic moment as earlier reported [27]. The estimated field-dependent refrigeration capacity [$\mathrm{RC} = \int_{T_{\rm cold}}^{T_{\rm hot}} |\Delta S(T)| dT$, where $T_{\rm cold}$ and $T_{\rm hot}$ represent the temperatures where the maximum value of ΔS is half below and above the $\Delta S(T)$ peak, respectively] for different applied p is shown in Fig. 3(c). The observed RC at ambient pressure is identical to that reported earlier for MnSi [17]. With application of $p = 9.6$ kbar, a small decrease of the RC (about 9% for $\Delta B = 7$ T with RC = 100.83 and 91.37 J/kg for $p = 0$ and 9.6 kbar, respectively) has been observed with respect to the ambient pressure value.

Finally, the magnetic phase diagram of MnSi for $p = 0$ kbar has been generated from ac-susceptibility data by adopting the approach described in Ref. [11], which is shown in Fig. 4(a). The associated first-order phase transition boundaries have been compared as derived from the field exponent $n(T, B)$. The critical magnetic fields ($B_{\rm c1}$, $B_{\rm A1}$, $B_{\rm A2}$, $B_{\rm c2}$) and temperatures ($T_{\rm A1}$, $T_{\rm A2}$, $T_{\rm c2}$) associated with the magnetic phase transitions have been obtained from ac-susceptibility data as defined in Refs. [11] and [31]. Some of the representative plots are shown in Figs. 4(b)–4(e). More details of the ac-susceptibility data are presented in

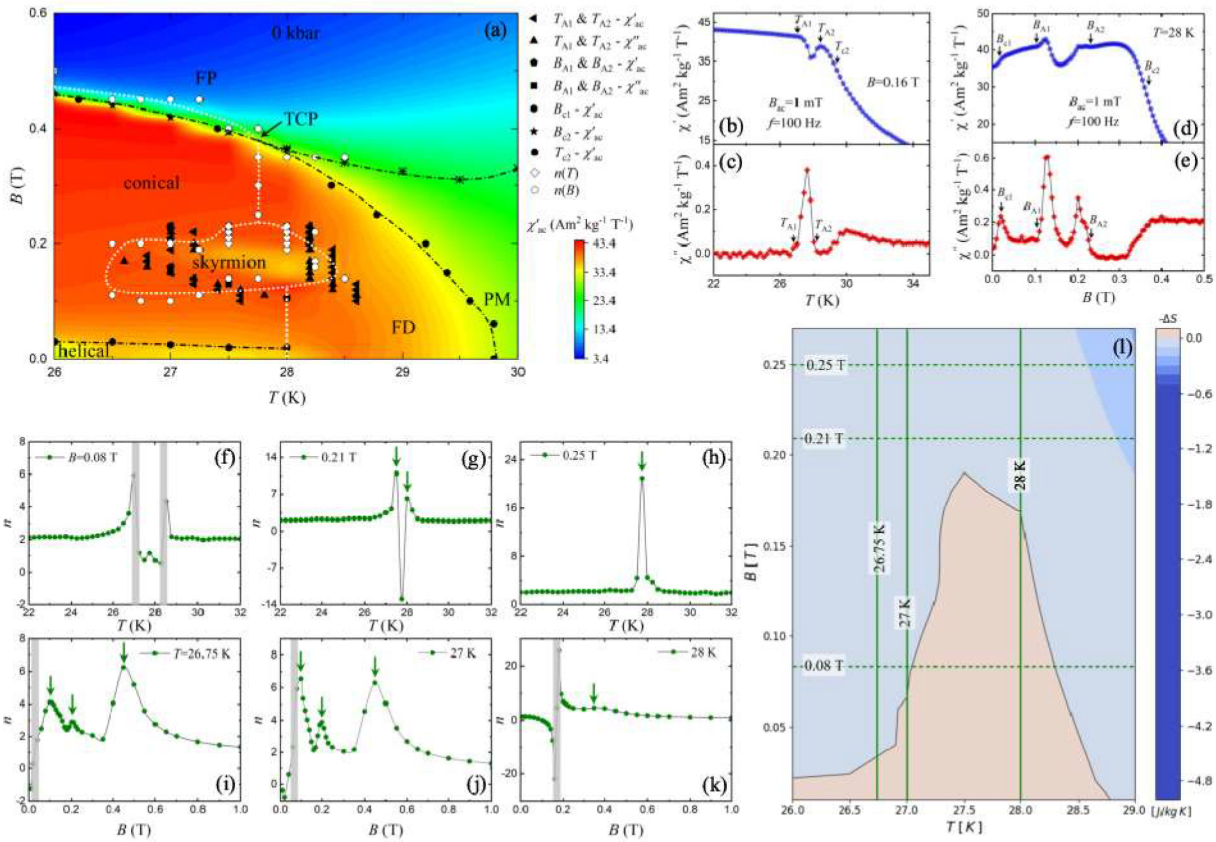

FIG. 4. (a) Magnetic phase diagram of MnSi generated using the ac-susceptibility data and the field-exponent of isothermal entropy change $n(T, B)$. χ' and χ'' are the real and imaginary part of the ac-susceptibility, respectively. (b) χ' and (c) χ'' as a function of temperature for $B = 0.16$ T. Field dependence of (d) χ' and (e) χ'' at $T = 28$ K. Temperature-dependent variation of n for the field values (f) $B = 0.08$ T, (g) $B = 0.21$ T, and (h) $B = 0.25$ T, respectively. Field dependence of n at (i) $T = 26.75$ K, (j) $T = 27$ K, and (k) $T = 28$ K, respectively. The vertical arrows indicate the peak position that corresponds to the first-order phase transition ($n > 2$). The peak that falls in the shaded region is forbidden due to the coincidence of peak position with zero crossover in $\Delta S(T, B)$. (l) The zero-crossover region in $\Delta S(T, B)$ is shown.

the Supplemental Material (S2 and S3) [28]. Depending on temperature and magnetic field, different types of ordered magnetic phases have been detected. The ordered magnetic phases, such as HM, conical, skyrmion, FD, and FP, have been identified based on earlier reports [5,7,10].

The estimation of n has been conducted by considering the following equation [21,32]:

$$n = \frac{d\ln|\Delta S|}{d\ln(B)}.$$

The isofield and isothermal variation of n for selected magnetic fields and temperatures are shown in Figs. 4(f)–4(h) and Figs. 4(i)–4(k), respectively, for $p = 0$ kbar [more details can be found in the Supplemental Material (S4) [28]]. Peaks with $n > 2$ have been detected in both $n(T)$ and $n(B)$. As observed in the present study and in agreement with earlier studies [18,20],

$\Delta S(T, B)$ is negative for a narrow region in the close vicinity of T_C for low magnetic fields during heating (equivalent to a decrease of magnetic field) and changes sign after crossing this region, as shown in Fig. 4(l). The zero-crossover in $\Delta S(T, B)$ is expected to create an associated signature in $n(T, B)$. It is therefore necessary to exclude the zero-crossover region from $n(T)$ and $n(B)$ [21,33]. One point that needs to be addressed here is that the skyrmion phase results in a field-induced (≡cooling) increase of entropy [18,20] and vice versa for decreasing magnetic field (≡heating). After the skyrmion phase transition to another phase (such as conical or FD), the associated changes in $\Delta S(T, B)$ can also result in a zero-crossover. The detection of the zero-crossover position was guided by the $\Delta S(T, B)$ contour plot [Fig. 4(l)]. The peak in $n(T)$ or $n(B)$ has been ignored when the peak point coincides with the zero-crossover position in the $\Delta S(T, B)$ plot [21,33]. For example, the peaks in $n(T)$ for $B = 0.08$ T [Fig. 4(f)] and in $n(B)$ at $T = 28$ K [Fig. 4(k)] have been disregarded due to the coincidence of the peak position in $n(T)$ or $n(B)$ with the zero-crossover in $\Delta S(T, B)$. The peak positions with $n > 2$ of the $n(T)$ and $n(B)$ curves correspond to the phase boundary of the first-order phase transition, which is also plotted in the magnetic phase diagram shown in Fig. 4(a). The first-order phase boundary derived from $n(T, B)$ is qualitatively similar to the phase boundary generated from ac-susceptibility and is also consistent with literature reports [5,7,10,11]. Interestingly, the skyrmion phase boundary is clearly visible in the phase diagram derived from $n(T, B)$. Moreover, combining ac-susceptibility data with $n(T, B)$, the tricritical point can be identified as previously indicated [6,10]. A minor discrepancy in the order of the phase transition between conical and FP

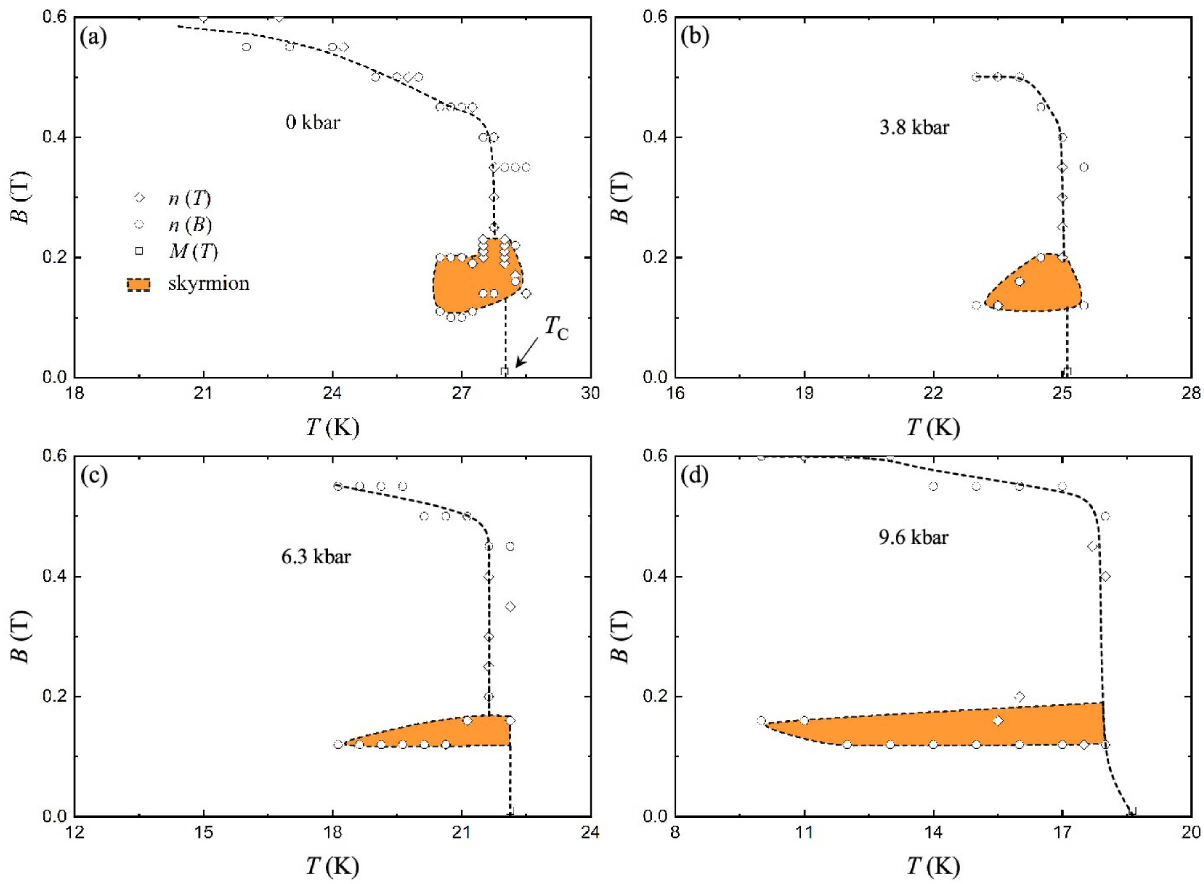

FIG. 5. Magnetic phase diagram of MnSi representing the first-order phase transition boundaries as generated using the field-exponent of isothermal entropy change $n(T, B)$ for the applied hydrostatic pressure (a) $p = 0$ kbar, (b) $p = 3.8$ kbar, (c) $p = 6.3$ kbar, and (d) $p = 9.6$ kbar, respectively. T_C at low field has been determined from $M(T)$ as measured for $B = 0.01$ T.

phases has been observed when compared to earlier reports where the phase boundary is generated from $n(T, B)$ [10]. The first-order conical-FP phase boundary derived from $n(T, B)$ is more extended towards low temperature. Despite that, the first-order phase transitions between skyrmion-conical/FD and conical-FD can be identified from $n(T, B)$.

The skyrmion phase boundaries generated from $n(T, B)$ are shown in Figs. 5(a)–5(d) for different applied hydrostatic pressures. A similar procedure to that adopted for *ambient pressure* has been used to generate the first-order phase transition boundaries for $p > 0$ [the details are included in the Supplemental Material (S5, S6, and S7) [28]]. As is evident in Fig. 5, the stabilization of the skyrmion phase persists up to the highest applied pressure, $p = 9.6$ kbar, which is consistent with earlier reports [34]. Narrower field and temperature steps of the isofield $M(T)$ measurements [as used to estimate ΔS and, therefore, $n(T, B)$ for $p = 0$ kbar] can increase the number of data points in the phase diagram for $p > 0$. The skyrmion phase is stable in a wider temperature range for higher applied pressures. Moreover, the first-order phase-transition boundaries between FD and other low-temperature magnetic phases (i.e., HM/skyrmion/conical phase) still exist up to the highest applied pressure, which is responsible for the sharp change in ΔS at T_C while maintaining a good MCE value for $p = 9.6$ kbar.

IV. CONCLUSION

In conclusion, the application of hydrostatic pressure on MnSi can simultaneously shift the phase-transition temperature near hydrogen liquefaction temperature while maintaining a relatively large MCE, which could have potential application for cryogenic magnetic refrigeration. The sharp change in ΔS at T_C just below the $\Delta S(T)$ peak and a curvature change in the $|\Delta S_{rev}|(B)$ plot at lower field observed for all p indicate that a long-range helical order and associated first-order transition at T_C still persists even at higher applied pressures of $p = 9.6$ kbar. Pressure-induced softening of the magnetic moment results in a larger ΔS at lower applied field, due to the characteristic change of magnetization under applied p. The most interesting outcome in the present study is that the field-exponent n of the isothermal entropy change has the potential to identify the complex first-order skyrmion phase transition as observed in the well-known skyrmion hosting MnSi system.

ACKNOWLEDGMENTS

This work was carried out in the framework of the Joint Lab BiBer and was supported by the Bundesministerium für Bildung und Forschung joint project

DiProMag—Digitalization of a process chain for the production, characterization, and prototypical application of magnetocaloric alloys, here the contribution of Bielefeld University: FKZ 13XP5 120B, with the objective of producing magnetocaloric Heusler compounds and ontology development.

DATA AVAILABILITY

The data that support the findings of this article are not publicly available upon publication because it is not technically feasible and/or the cost of preparing, depositing, and hosting the data would be prohibitive within the terms of this research project. The data are available from the authors upon reasonable request.

[1] S. Mühlbauer, B. Binz, F. Jonietz, C. Pfleiderer, A. Rosch, A. Neubauer, R. Georgii, and P. Böni, Skyrmion lattice in a chiral magnet, Science **323**, 915 (2009).

[2] R. Ritz, M. Halder, M. Wagner, C. Franz, A. Bauer, and C. Pfleiderer, Formation of a topological non-Fermi liquid in MnSi, Nature (London) **497**, 231 (2013).

[3] F. Büttner, I. Lemesh, and G. S. D. Beach, Theory of isolated magnetic skyrmions: From fundamentals to room temperature applications, Sci. Rep. **8**, 4464 (2018).

[4] A. Fert, V. Cros, and J. Sampaio, Skyrmions on the track, Nat. Nanotechnol. **8**, 152 (2013).

[5] J. Kindervater, T. Adams, A. Bauer, F. X. Haslbeck, A. Chacon, S. Mühlbauer, F. Jonietz, A. Neubauer, U. Gasser, G. Nagy, N. Martin, W. Häußler, R. Georgii, M. Garst, and C. Pfleiderer, Evolution of magnetocrystalline anisotropies in $Mn_{1-x}Fe_xSi$ and $Mn_{1-x}Co_xSi$ as inferred from small-angle neutron scattering and bulk properties, Phys. Rev. B **101**, 104406 (2020).

[6] L. Zhang, D. Menzel, C. Jin, H. Du, M. Ge, C. Zhang, L. Pi, M. Tian, and Y. Zhang, Critical behavior of the single-crystal helimagnet MnSi, Phys. Rev. B **91**, 024403 (2015).

[7] J. Kindervater, I. Stasinopoulos, A. Bauer, F. X. Haslbeck, F. Rucker, A. Chacon, S. Mühlbauer, C. Franz, M. Garst, D. Grundler, and C. Pfleiderer, Weak crystallization of fluctuating skyrmion textures in MnSi, Phys. Rev. X **9**, 041059 (2019).

[8] C. Pappas, E. Lelièvre-Berna, P. Falus, P. M. Bentley, E. Moskvin, S. Grigoriev, P. Fouquet, and B. Farago, Chiral paramagnetic skyrmion-like phase in MnSi, Phys. Rev. Lett. **102**, 197202 (2009).

[9] M. Janoschek, M. Garst, A. Bauer, P. Krautscheid, R. Georgii, P. Böni, and C. Pfleiderer, Fluctuation-induced first-order phase transition in Dzyaloshinskii-Moriya helimagnets, Phys. Rev. B **87**, 134407 (2013).

[10] A. Bauer, M. Garst, and C. Pfleiderer, Specific heat of the skyrmion lattice phase and field-induced tricritical point in MnSi, Phys. Rev. Lett. **110**, 177207 (2013).

[11] A. Bauer and C. Pfleiderer, Magnetic phase diagram of MnSi inferred from magnetization and ac susceptibility, Phys. Rev. B **85**, 214418 (2012).

[12] X. Z. Yu, Y. Onose, N. Kanazawa, J. H. Park, J. H. Han, Y. Matsui, N. Nagaosa, and Y. Tokura, Real-space observation of a two-dimensional skyrmion crystal, Nature (London) **465**, 901 (2010).

[13] M. Soda, E. M. Forgan, E. Blackburn, E. Campillo, V. Ryukhtin, I. Hoffmann, A. Kikkawa, Y. Taguchi, H. Yoshizawa, and H. Kawano-Furukawa, Asymmetric slow dynamics of the skyrmion lattice in MnSi, Nat. Phys. **19**, 1476 (2023).

[14] A. Neubauer, C. Pfleiderer, B. Binz, A. Rosch, R. Ritz, P. G. Niklowitz, and P. Böni, Topological Hall effect in the a phase of MnSi, Phys. Rev. Lett. **102**, 186602 (2009).

[15] Y. Chai, P. Lu, H. Du, J. Shen, Y. Ma, K. Zhai, L. Wang, Y. Shi, H. Li, W. Wang, and Y. Sun, Probe of skyrmion phases and dynamics in MnSi via the magnetoelectric effect in a composite configuration, Phys. Rev. B **104**, L100413 (2021).

[16] S. Wang, Y. Hu, J. Tang, W. Wei, J. Cong, Y. Sun, H. Du, and M. Tian, Magnetostriction of helimagnets in the skyrmion crystal phase, New J. Phys. **21**, 123052 (2019).

[17] P. Arora, M. K. Chattopadhyay, and S. B. Roy, Magnetocaloric effect in MnSi, Appl. Phys. Lett. **91**, 062508 (2007).

[18] M. Ge, L. Zhang, D. Menzel, H. Han, C. Jin, C. Zhang, L. Pi, and Y. Zhang, Scaling investigation of the magnetic entropy change in helimagnet MnSi, J. Alloys Compd. **649**, 46 (2015).

[19] T. Samanta, I. Das, and S. Banerjee, Giant magnetocaloric effect in antiferromagnetic $ErRu_2Si_2$ compound, Appl. Phys. Lett. **91**, 152506 (2007).

[20] C. Dhital and J. F. DiTusa, Entropic signatures of the skyrmion lattice phase in $MnSi_{1-x}Al_x$ and $Fe_{1-y}Co_ySi$, Phys. Rev. B **102**, 224408 (2020).

[21] J. Y. Law, V. Franco, L. M. Moreno-Ramírez, A. Conde, D. Y. Karpenkov, I. Radulov, K. P. Skokov, and O. Gutfleisch, A quantitative criterion for determining the order of magnetic phase transitions using the magnetocaloric effect, Nat. Commun. **9**, 2680 (2018).

[22] C. Pfleiderer, D. Reznik, L. Pintschovius, H. v. Löhneysen, M. Garst, and A. Rosch, Partial order in the non-Fermi-liquid phase of MnSi, Nature (London) **427**, 227 (2004).

[23] C. Pfleiderer, P. Böni, T. Keller, U. K. Rößler, and A. Rosch, Non-Fermi liquid metal without quantum criticality, Science **316**, 1871 (2007).

[24] J. Rodríguez-Carvajal, *Introduction to the Program FULLPROF: Refinement of Crystal and Magnetic Structures From Powder and Single Crystal Data* (Laboratoire Léon Brillouin, CEA/Saclay, 2015).

[25] A. Eiling and J. S. Schilling, Pressure and temperature dependence of electrical resistivity of Pb and Sn from 1–300 K and 0–10 GPa-use as continuous resistive pressure monitor accurate over wide temperature range; superconductivity under pressure in Pb, Sn and In, J. Phys. F **11**, 623 (1981).

[26] L. Caron, N. B. Doan, and L. Ranno, On entropy change measurements around first order phase transitions in caloric materials, J. Phys.: Condens. Matter **29**, 075401 (2017).

[27] L. J. Bannenberg, R. Sadykov, R. M. Dalgliesh, C. Goodway, D. L. Schlagel, T. A. Lograsso, P. Falus, E. Lelièvre-Berna, A. O. Leonov, and C. Pappas, Skyrmions and spirals in MnSi under hydrostatic pressure, Phys. Rev. B **100**, 054447 (2019).

[28] See Supplemental Material at http://link.aps.org/supplemental/10.1103/1ftc-3xyw for the details of the variation of $\Delta S(T)$ for all applied fields up to $\Delta B = 7$ T and pressure up to $p =$ 9.6 kbar, ac-susceptibility as afunction of temperature and dc

magnetic field, $\Delta S(T, B)$ color contour plots for different pressures highlighting zero crossover, and the peak positions in $n(T)$ and $n(B)$ associated with the first-order phase transition for different applied p.

[29] V. K. Pecharsky and K. A. Gschneidner, Jr., Magnetocaloric effect from indirect measurements: Magnetization and heat capacity, J. Appl. Phys. **86**, 565 (1999).

[30] W. Liu, T. Gottschall, F. Scheibel, E. Bykov, N. Fortunato, A. Aubert, H. Zhang, K. Skokov, and O. Gutfleisch, Designing magnetocaloric materials for hydrogen liquefaction with light rare-earth Laves phases, J. Phys. Energy **5**, 034001 (2023).

[31] T. Y. Ou-Yang, G. J. Shu, C. D. Hu, and F. C. Chou, Dynamic susceptibility study on the skyrmion phase stability of $Fe_{0.7}Co_{0.3}Si$, J. Appl. Phys. **117**, 123903 (2015).

[32] T. D. Shen, R. B. Schwarz, J. Y. Coulter, and J. D. Thompson, Magnetocaloric effect in bulk amorphous $Pd_{40}Ni_{22.5}Fe_{17.5}P_{20}$ alloy, J. Appl. Phys. **91**, 5240 (2002).

[33] J. Y. Law, Á. Díaz-García, L. M. Moreno-Ramírez, V. Franco, A. Conde, and A. K. Giri, How concurrent thermomagnetic transitions can affect magnetocaloric effect: The $Ni_{49+x}Mn_{36-x}In_{15}$ Heusler alloy case, Acta Mater. **166**, 459 (2019).

[34] R. Ritz, M. Halder, C. Franz, A. Bauer, M. Wagner, R. Bamler, A. Rosch, and C. Pfleiderer, Giant generic topological Hall resistivity of MnSi under pressure, Phys. Rev. B **87**, 134424 (2013).